



Effect of mesoporous silica topology on the formation of active sites in copper supported catalysts for methanol decomposition

Tanya Tsoncheva^{a,*}, Izabela Genova^a, Mariana Stoyanova^b, Marga-Martina Pohl^b, Radostin Nickolov^c, Momtchil Dimitrov^a, Eva Sarcadi-Priboczki^d, Mihail Mihaylov^e, Daniela Kovacheva^e, Konstantin Hadjiivanov^e

^a Institute of Organic Chemistry with Centre of Phytochemistry, Bulgarian Academy of Sciences, Sofia, Bulgaria

^b Leibniz-Institut für Katalyse e.V. an der Universität Rostock (LIKAT), Rostock, Germany

^c University of Chemical Technology and Metallurgy, Sofia, Bulgaria

^d Institute of Nuclear Research, Hungarian Academy of Sciences, Debrecen, Hungary

^e Institute of General and Inorganic Chemistry, Bulgarian Academy of Sciences, Sofia, Bulgaria

ARTICLE INFO

Article history:

Received 8 July 2013

Received in revised form

20 September 2013

Accepted 3 October 2013

Available online 12 October 2013

Keywords:

Supported copper nanoparticles

Mesoporous silica

Preparation method

Methanol decomposition

ABSTRACT

Modified incipient wetness impregnation procedure was applied for deposition of finely dispersed CuO or metallic copper particles into ordered mesoporous silica host matrix (KIT-6 and SBA-15). This modified procedure consists of number of consecutive impregnation steps with copper nitrate solution with changeable concentration and soft drying under vacuum procedures. Nitrogen physisorption, XRD, UV-vis, TEM-EDXS, FTIR of probe molecules (CO, NO and N₂) and TPR were applied for characterization of copper state in the matrix. The obtained materials were tested as catalysts in methanol decomposition. Selected catalytic experiments were carried out under very low coverage of the surface with ¹¹C-radiolabelling methanol. In situ FTIR study of methanol decomposition was also performed. It was found that the catalytic behaviour of copper, supported on mesoporous materials, depends in a complex way on the dispersion and accessibility of copper species within the host matrix. They can be tuned by copper loading and pore topology of the support. The optimal catalytic activity in methanol decomposition is achieved at about 8 and 15 wt.% copper content for the SBA-15 and KIT-6 mesoporous supports, respectively.

© 2013 Elsevier B.V. All rights reserved.

1. Introduction

Recently, hydrogen and hydrogen-rich gases have attracted much attention as promising alternative source of energy for fuel cells and low-emission automobile applications [1–6]. On-board production of hydrogen from a liquid fuel is considered as a good alternative due to safety storage and no requirement of new automobile infra-structures. Methanol is one of the best candidates, because it could convert into hydrogen at relatively low temperatures via catalytic decomposition, steam reforming or autothermal reforming processes with high efficiency due to its high hydrogen to carbon ratio. In last decade, the interest to methanol significantly increased due to the possibility to obtain methanol from renewable sources such as biomass, waste products or carbon dioxide from the atmosphere. Many studies were performed on dehydrogenation of methanol over copper containing catalysts, especially on the catalysts of methanol synthesis. However, Cheng et al. [7,8]

established that the conventional Cu/ZnO based methanol synthesis catalysts had good initial activity in methanol decomposition reaction was quickly deactivated. They reported that Ba, Si and Mn oxides promoted the activity of copper catalysts, while Cr oxides improved their stability [7]. The role of CO₂ for stabilization of the activity of Cu based catalysts was also reported in [8]. Up to now, much effort has been attached to control the behaviour of copper catalysts via understanding the nature of the catalytic sites and mechanism of the reaction [9 and refs. therein]. Millar et al. [10] demonstrated that methanol adsorption on Cu/SiO₂ resulted in the formation of methoxide groups, which after heating, transformed to CO₂ and CO via methyl formate. Clarke et al. [11] confirmed the formation of adsorbed methoxide, formaldehyde, methylenebisoxo, and formate groups on copper. Latter, Fisher and Bell [12] reported that depending on the presence of methanol in the gas phase, surface methoxide species could decompose either to CO₂ and H₂ via formaldehyde and formate intermediates or to CO and H₂ via methyl formate ones. It was found that the formation of methyl formate intermediate from methanol showed low sensitivity to the state of metal copper, while its further decomposition to CO and hydrogen depends on the state of metal copper in

* Corresponding author. Tel.: +359 029796 640.

E-mail address: tsoncheva@orgchm.bas.bg (T. Tsoncheva).

the catalysts [7,13]. Greeley and Mavrikakis [14] demonstrated that the abstraction of single hydrogen atom from methoxide species was the rate-limiting step in the reaction. Minyukova et al. [13] assumed that the methyl formate selectivity could be close to 1 at low methanol conversion but the selectivity decreased with the conversion increase. Many authors believed that all three copper states, Cu^{2+} , Cu^+ , and Cu^0 , are active in methanol decomposition [13], but Domokos et al. [15] and Morikawa [16] concluded that only Cu^{2+} ions are responsible for the dehydration of methanol to methyl formate, while Guerreiro et al. [17] assumed Cu^0 instead of Cu^{2+} as active site. Guerreiro et al. [18] stressed on the critical limit of copper particle size which can ensure methanol dehydrogenation. However it was found that the amount of supported copper had a strong effect on the catalyst efficiency and the state of active phase could be modified in a wide range by the preparation method used [19 and refs. therein]. The application of direct synthesis technique typically results in relatively low copper loading, while the traditional impregnation method [20–22] usually provides agglomeration of copper species on the silica surface, especially at high metal content. Chen et al. [23] found that the grafting method resulted predominantly in the formation of Cu^+ ions, while a partial destruction of support structure occurred when homogeneous deposition precipitation method was used. The predominant formation of oligomeric Cu–O–Cu species was found by molecular design method, while isolated Cu^{2+} ions dominated by the impregnation method [24]. Recently, mesoporous silica revealed good prospects as a host matrix of tunable nanoscale metal/metal oxide particles due to their unequal pore structure characteristics [24–27 and refs. therein]. In our previous study we demonstrated better copper dispersion of copper loaded on hexagonal MCM-41 compared to cubic MCM-48 mesoporous silica [28], while negligible effect of pore structure on the state of copper species has been established when copper precursor strongly interacted with the surface functionality [29]. Patel et al. [30] supposed that for the copper catalysts prepared by impregnation technique, the pore volume and surface area of mesoporous silica supports had a lower dominance on the copper dispersion than the pore topology.

The aim of the current investigation is to prepare copper supported mesoporous silica catalysts for methanol decomposition varying the copper loading in a wide range (1.5–25 wt.%) by simple modification of the traditional incipient wetness impregnation technique. This modified technique includes “step-wise” loading of copper phase by number of consecutive impregnations with copper nitrate solution with changeable concentration followed by soft drying procedure under vacuum. Mesoporous silica type SBA-15 and KIT-6, which structures represent ordered cylindrical mesopores, arranged in hexagonal and cubic symmetry respectively, are compared as host matrices [31,32]. Nitrogen physisorption, XRD, UV-vis, TEM–EDXS, FTIR of probe molecules (CO, NO and N_2) and H_2 -TPR were applied for the characterization of the copper state. In order to highlight the state of copper active sites more precisely, ^{11}C -methanol radiolabelling technique and in situ FTIR study of methanol conversion were applied.

2. Experimental

2.1. Materials

Mesoporous silica type SBA-15 and KIT-6 were synthesized using tetraethylorthosilicate (TEOS) as a silica source and Pluronic P123 triblock-co-polymer (EO20PO70EO20) as structure-directing agent according to the procedures described in [31,32], respectively. A series of copper modifications of these silicas were prepared by modified incipient wetness impregnation technique

(MWI). The method included “step-wise” copper deposition by alternating sequence of number incipient wetness impregnation and vacuum drying cycles. Aqueous solution of copper nitrate was used as a precursor. The concentration of the impregnated solutions, the number of “impregnation-drying” cycles and the drying temperature were varied and the data for the procedures are summarized in Table 1. Samples with copper loading in the range of 1.5–25 wt.% were obtained (Table 1). For comparison, selected samples containing 8 wt.% Cu were prepared using conventional one-step incipient wetness impregnation technique (WI). The precursor was decomposed after calcination in air at 763 K for 2 h. The samples were denoted as $x\text{CuO/S}$, where x was the copper content (as wt.%) and S was SBA-15 or KIT-6 support. Separately, portions of the modifications thus obtained were reduced in a flow of 50 vol.% H_2 in Ar at 523 K for 2 h and the obtained reduced samples thus obtained were denoted as $x\text{Cu/S}$. For comparison, the studied catalysts were compared to a commercial copper catalyst for low-temperature water gas shift reaction (Haldor Topsøe), denoted as CC.

2.2. Methods of catalyst characterization

The specific surface area (S_{BET}) and porosity of the materials were calculated from nitrogen adsorption–desorption isotherm collected at 77 K on a BELSORB-mini II apparatus (BEL Japan Inc.) Prior to the measurements, the samples were outgassed for 2 h at 250 °C. S_{BET} was calculated applying the Brunauer, Emmet and Teller (BET) equation for N_2 relative pressure in range of $0.05 < P/P_0 < 0.30$. Pore size distribution was determined by Barrett–Joyner–Halenda (BJH) method from the desorption branch of the isotherm. Powder X-ray diffraction patterns were collected within the range of 5.3–80.0° 2θ on a Bruker D8 Advance diffractometer with $\text{Cu K}\alpha$ radiation and using a LynxEye detector. Low-angle part of the patterns was collected from 0.3° to 8.0° 2θ using the knife-edge anti-scatter screen attachment of the primary beam. The average crystallite size was evaluated according to Scherrer equation.

The UV-vis spectra were recorded on Jasco V-650 UV-vis spectrophotometer equipped with a diffuse reflectance unit.

The TEM measurements were performed at 200 kV with an aberration-corrected JEM-ARM200F (JEOL, Corrector: CEOS), equipped with a JED-2300 (JEOL) energy-dispersive X-ray-spectrometer (EDXS) for chemical analysis. The aberration corrected STEM imaging High-Angle Annular Dark Field (HAADF) and Annular Bright Field (ABF) were performed with a spot size of approximately 0.1 nm, probe current of 120 pA, convergence angle of 30–36° and collection semi-angles for HAADF and ABF of 90–170 mrad and 11–22 mrad, respectively. The sample was deposited without any pretreatment on a holey carbon supported Ni-grid (mesh 300) and transferred to the microscope.

FTIR spectra in the region of skeletal vibrations were recorded on a Bruker Vector 22 spectrometer at a resolution of 1–2 cm^{−1}, accumulating 64–128 scans and KBr pellets technique.

FTIR spectra of probe molecules were recorded with a Nicolet 6700 spectrometer accumulating 64 scans at a spectral resolution of 2 cm^{−1}. Self-supporting pellets (ca. 10 mg cm^{−2}) were prepared from the powdered samples and treated in situ in a purpose-made IR cell allowing measurements at ambient and lower temperature. The cell was connected to a vacuum-adsorption apparatus with a residual pressure below 10^{-3} Pa. Prior to the adsorption of probe molecules, the samples were activated by calcination in air at 673 K for 1 h and evacuation at 723 K for 1 h. Reduced samples were obtained by flowing with H_2 (10 kPa) at 523–723 K for 1 h followed by evacuation at 673 K. Samples treated with methanol (for details see below) were also characterized in situ. The experiments on adsorption of probe molecules (CO, NO and N_2) were performed at

Table 1

Samples composition, MWI procedure ($C_{\text{Cu}(\text{NO}_3)_2}$ – concentration of impregnation solution, N – number of “impregnation-drying” steps, T_d – drying temperature, T_t /atm – temperature of activation and activation atmosphere), average particle size (D^a and D^b) and specific activity (SA) in methanol decomposition at 650 K.

Sample	Cu (wt.%)	$C_{\text{Cu}(\text{NO}_3)_2}$ (wt.%)	N	T_d (K)	T_t (K/atm)	$D_{\text{CuO/Cu}}$ (nm) ^a	D_{Cu} (nm) ^b	SA
1.5CuO/KIT-6	1.5	1.5	2	343	763/air			36.0
1.5Cu/KIT-6	1.5				523/H ₂			42.0
1.5CuO/SBA-15	1.5	1.5	2	343	763/air			30.0
1.5Cu/SBA-15	1.5				523/H ₂			30.0
4CuO/KIT-6	4.0	4	2	343	763/air	36.5		15.8
4Cu/KIT-6	4.0				523/H ₂			15.0
4CuO/SBA-15	4.0	4	2	343	763/air		1.5	14.2
4Cu/SBA-15	4.0				523/H ₂			14.2
8CuO/KIT-6	8.0	4	4	343	763/air	40.4		7.5
8Cu/KIT-6	8.0				523/H ₂	47.6		8.0
8Cu/KIT-6(cat)	8.0				523/H ₂ and catalysis	56.1	0.9	
8CuO/SBA-15	8.0	4	4	343	763/air	41.8		9.2
8Cu/SBA-15	8.0				523/H ₂	40.1	1.9	9.0
8Cu/SBA-15(cat)	8.0				523/H ₂ and catalysis	45.8		
15CuO/KIT-6	15.0	5	6	363	763/air	38.3		4.5
15Cu/KIT-6	15.0				523/H ₂			5.0
15CuO/SBA-15	15.0	5	6	363	763/air	35.5		3.4
15Cu/SBA-15	15.0				523/H ₂		2.0	4.3
25CuO/KIT-6	25.0	5	10	363	763/air	33.8		2.5
25Cu/KIT-6	25.0				523/H ₂			2.5
25CuO/SBA-15	25.0	5	10	363	763/air	27.2		2.2
25Cu/SBA-15	25.0				523/H ₂			2.2

^a $D_{\text{CuO/Cu}}$ – average CuO or Cu particles diameter elucidated by XRD.

^b D_{Cu} – average Cu particles diameter elucidated by TEM.

100 K or at ambient temperature. Carbon monoxide (>99.5% purity) was supplied by Merck. Nitrogen monoxide (>99.5%) and nitrogen (99.999%) were purchased from Messer.

The TPR/TG (temperature-programmed reduction/thermogravimetric) analyses were performed on a Setaram TG92 instrument in a flow of 50 vol.% H₂ in Ar (100 cm³ min⁻¹) and heating rate of 5 K min⁻¹.

2.3. Catalytic investigation

Methanol conversion was carried out in a flow reactor (0.055 g of catalyst), argon being used as a carrier gas (50 cm³ min⁻¹). The methanol partial pressure was 1.57 kPa. The catalysts were tested under conditions of a temperature-programmed regime within the range of 350–770 K with heating rate of 1 K min⁻¹. Selected experiments were performed under isothermal conditions at 650 K. On-line gas chromatographic analyses were performed on HP apparatus equipped with flame ionization and thermoelectric conductivity detectors, on a PLOT Q column, using an absolute calibration method and a carbon based material balance. The product selectivity was calculated as $Y_i/X \times 100$, where Y_i was the yield of the i product (calculated as detected amount of i product/initial amount of methanol, before the introduction in the catalytic reactor) and X was the methanol conversion at selected temperature. Specific activity (SA) was calculated as X/m_i where X and m_i were the conversion at 650 K and copper content in the sample (wt.%), respectively. ¹¹C-methanol radiolabelling experiments were done in a closed static reactor and the analyses were performed on HP 6890 GC equipped with a PLOT Q column, flame ionization detector (FID) and radioisotope detector BIOSCAN Flow-Count (RD). Before the catalytic test calcined samples were treated under Ar flow at 373 K for 1 h. The reduction of the samples was performed in situ in a flow of H₂ and Ar (1:1) at 523 K for 2 h. The catalytic experiments were carried out after preliminary coverage of the catalyst surface with ¹²C- and ¹¹C-methanol according to the following adsorption procedures:

(A) ¹²C-methanol adsorption followed by flushing with He and adsorption of ¹¹C-methanol, all this at 333 K.

(B) ¹²C-methanol adsorption at 333 K, further heating to 373 K and flushing with He 373 K, then cooling to 333 K and adsorption of ¹¹C-methanol.

After the pre-adsorption procedures, the catalytic experiments were carried out under the conditions of step-wise temperature increase.

Methanol decomposition experiments were performed in static conditions in the IR cell following the gas phase composition by FTIR spectroscopy. Similarly to the other catalytic tests, before the experiments the calcined samples were (i) evacuated at 373 K for 1 h or (ii) reduced with H₂ at 523 K for 1 h and evacuated at the same temperature. Methanol (2 kPa equilibrium pressure) was introduced to the catalysts at ambient temperature. Then the system was heated to 723 K and methanol allowed to interact with the sample for 15 min at this temperature. Then the gas phase was pumped out at the same temperature. The procedure was repeated and then the catalysts were characterized by IR spectroscopy of probe molecules.

3. Results and discussion

3.1. Catalytic tests

3.1.1. Methanol decomposition

The temperature dependencies of methanol decomposition on different catalysts in a flow type reactor are presented in Fig. 1. Methanol conversion is typically observed above 550–570 K and carbon monoxide is the main registered carbon-containing product, but methyl formate (up to 10–14%), CO₂ (up to 9–10%), methane (up to 2–3%) and dimethyl ether (DME) (up to 1–3%) are also detected as by-products. Hydrogen was released in stoichiometric amount in accordance with Eq. (1). Carbon based balance for the products distribution was done. For simplicity, the selectivity

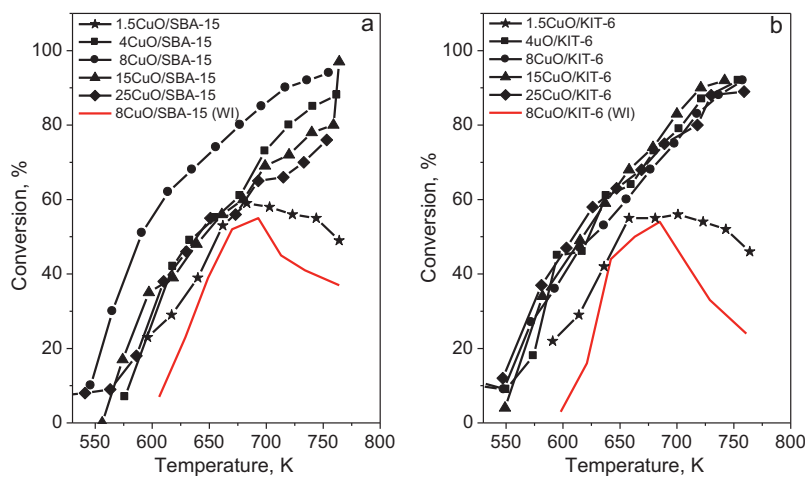


Fig. 1. Methanol decomposition vs. temperature on various SBA-15 (a) and KIT-6 (b) modifications prepared by MWI method. For comparison 8CuO/SBA-15(WI) and 8CuO/KIT-6(WI) modifications prepared by conventional impregnation technique are presented.

to CO is only presented in Fig. S1, because it provides valuable information for the catalysts behaviour in the main process of hydrogen production via methanol decomposition according to Eq. (1) [13]:



Supplementary material related to this article can be found, in the online version, at <http://dx.doi.org/10.1016/j.apcatb.2013.10.002>.

For most of the modifications, the conversion increases with the temperature and reaches 90–100% at 750 K. The appearance of well defined maximum of about 60% conversion at 675 K is observed only for both 1.5% CuO/S materials. All other KIT-6 modifications exhibit close catalytic activity despite the copper loading increase in the range of 4–25 wt.%. Typically the KIT-6 modifications decompose methanol to CO with higher activity compared to their SBA-15 counterparts. Among the studied materials, 8CuO/SBA-15 exhibits the highest catalytic activity (Fig. 1). However, the complex course of the conversion with increasing the temperature urge the authors to assume changes in the catalysts during the reaction. This assumption is well demonstrated with the behaviour of the samples under isothermal conditions (Fig. S2). For example, about 1.5 and 2 times decrease of the catalytic activity was observed during 3 h time on stream at 650 K for 8CuO/SBA-15 and 8CuO/KIT-6, respectively. For comparison, tested under these conditions the commercial catalyst exhibits about 1.5 times higher initial catalytic activity which after 3 h decreases more than 3 times. Thus, the formation of active copper phase seems to be realized not only during the preparation procedure but also during the reaction by the influence of the reaction medium and it is affected by pore topology of the mesoporous host matrix. In order to compare the samples more precisely we normalized the conversion per 1 wt.% Cu content (see SA values in Table 1). Again, with the exception of the samples containing 8 wt.% Cu prepared by MWI technique, KIT-6 copper modifications are characterized with higher specific activity as compared to SBA-15 analogues. Note that for each silica support SA significantly decreases with copper content increase from 1.5 to 25 wt.% indicating changes with the state of active phase with copper loading increase. The conversion curves of the samples prepared by conventional incipient wetness impregnation method (8CuO/S (WI)) are shifted to higher temperatures as compared to the analogues prepared by the MWI and started to deactivate after reaching a maximum of about 50% at 680 K.

Supplementary material related to this article can be found, in the online version, at <http://dx.doi.org/10.1016/j.apcatb.2013.10.002>.

In order to diminish the impact of the reduction of copper phase by the reaction medium, catalytic experiments with samples preliminary reduced in situ by hydrogen were performed. The temperature dependencies of methanol conversion and CO selectivity are presented in Fig. 2 and Fig. S3, respectively. The calculated SA values are listed in Table 1. Similarly to the calcined materials, under isothermal conditions the reduced samples demonstrate a decrease in catalytic activity with time on stream (Fig. S2). The complex changes in the shape of conversion curves as well as the absence of clear effect of reduction pre-treatment on the SA values (Table 1, Fig. 2) strongly indicate that the catalytic behaviour of the samples is affected not only by the copper oxidation state but by the dispersion, location and flexibility of copper phase into the porous matrix as well. Note the different course of the conversion curves for the reduced 1.5 Cu/S samples as compared to their oxidized analogues (Fig. S4). This point will be discussed further on in details (see Sections 3.1.3 and 3.2.7).

Supplementary material related to this article can be found, in the online version, at <http://dx.doi.org/10.1016/j.apcatb.2013.10.002>.

3.1.2. ^{11}C -radioactive isotope labelling study of methanol decomposition

As was illustrated in Fig. 1, the samples 8CuO/S differ significantly in their catalytic behaviour. In order to obtain more information for the state of copper phase with respect to the differences in the support pore topology, catalytic experiments with ^{11}C -radiolabelling methanol were performed in a closed catalytic reactor under traces of $^{11}\text{CH}_3\text{OH}$ coverages of the solid surface. The variations in the degree of surface coverages with $^{11}\text{CH}_3\text{OH}$ were achieved by original pre-treatment procedures, which include partial blocking of the active surface with $^{12}\text{CH}_3\text{OH}$ (Fig. 3). According to the procedure A, $^{12}\text{CH}_3\text{OH}$ was adsorbed at 333 K and after flushing with He, adsorption of $^{11}\text{CH}_3\text{OH}$ was carried out at the same temperature. We expect that this procedure provides predominant adsorption of $^{11}\text{CH}_3\text{OH}$ on the accessible weak adsorption sites, while the others remain blocked with $^{12}\text{CH}_3\text{OH}$ (Fig. 3a). Under the procedure B, $^{12}\text{CH}_3\text{OH}$ was adsorbed at 333 K and after further temperature increase up to 373 K and flushing with He at 373 K, the sample was cooled again to 333 K and then $^{11}\text{CH}_3\text{OH}$ was adsorbed. It is reasonable that procedure B provides ^{12}C -methanol adsorption only on small portion of the strongest adsorption sites and, hence, higher coverage of the surface with $^{11}\text{CH}_3\text{OH}$ (Fig. 3b) in comparison with the procedure A with a predominant location of $^{11}\text{CH}_3\text{OH}$ on the weak and partially on the stronger sites is expected.

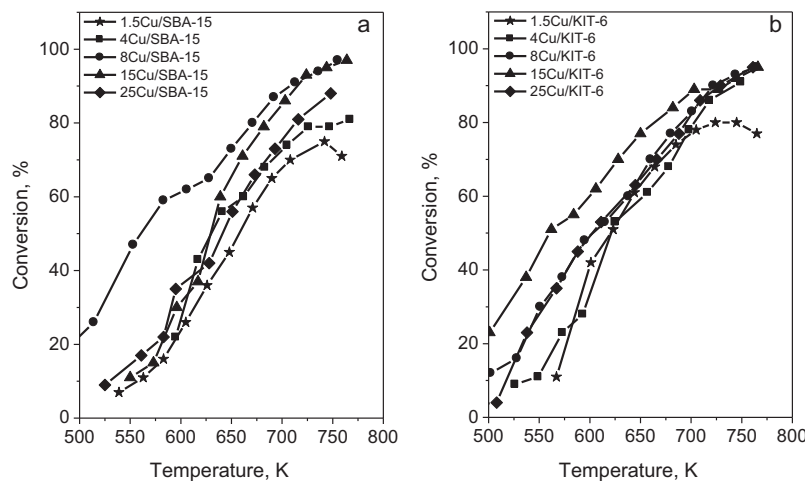


Fig. 2. Methanol decomposition vs. temperature on various reduced in hydrogen SBA-15 (a) and KIT-6 (b) modifications, prepared by MWI method.

In contrast to the experiments in the conventional flow reactor (see above), here the primary observed product from methanol decomposition is $^{11}\text{CO}_2$. The observed results urged the authors to assume a mechanism (**Scheme 1**), including formation of surface methoxide species (route 1) and their transformation to aldehyde ones (route 2) as the first step of methanol interaction with the surface. Further, with the participation of oxygen from the solid the surface aldehyde intermediates convert to dioxymethylene (route 3) and formate ones (route 4), which finely decompose to CO_2 [33,34 and refs. therein]. The catalytic activity for both 8CuO/S materials increases with the increase of surface coverage with ^{11}C -methanol, which is realized during the *procedure B* (Fig. 3b). Under these conditions, higher conversion is registered for 8CuO/SBA-15 as compared to 8CuO/KIT-6, which is in agreement with the test in the flow reactor (see above). This evidences presence of larger portion of strong adsorption sites for the former material. The observed features could be associated with higher dispersion and/or better accessibility of copper species in 8CuO/SBA-15 as compared to 8CuO/KIT-6. We repeated the catalytic experiments on the catalyst, which was already used in the catalytic test (Fig. 3a, curve 3). Note that this

used catalyst represents higher catalytic activity as compared to the fresh one, which indicates changes in the state of active phase under the reaction medium.

3.1.3. *In situ* FTIR study of methanol decomposition

Let us recall one interesting result from the conventional catalytic test (Fig. S4). Methanol conversion on the 1.5CuO/S catalysts increases up to 680 K and starts to decrease above this temperature. As was reported in Section 3.1.1, a different catalytic curve has been observed for the sample reduced in situ with H_2 before the test. In this case the conversion increases up to 750 K, i.e., above 680 K, the reduced sample shows a higher catalytic activity than the calcined one. To verify this result we performed catalytic test under static conditions in the infrared cell (closed reactor) following the gas phase composition by FTIR spectroscopy. Methanol was introduced to the system at room temperature and then the catalyst heated at 723 K for 15 min. At these conditions the reaction almost stops after ca. 15 min. Fig. 4 shows the IR spectra of the gas phase before and after interaction with the oxidized and reduced 1.5Cu/KIT-6 samples with methanol vapour at 723 K for 15 min.

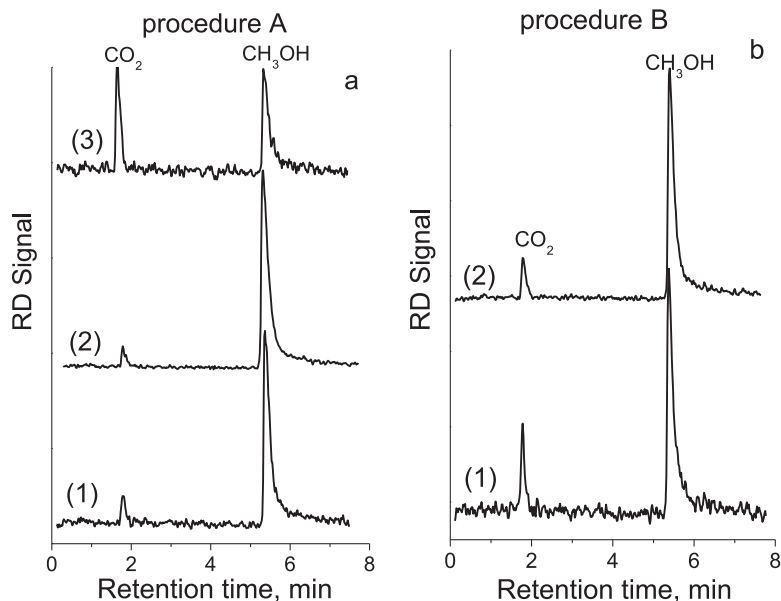
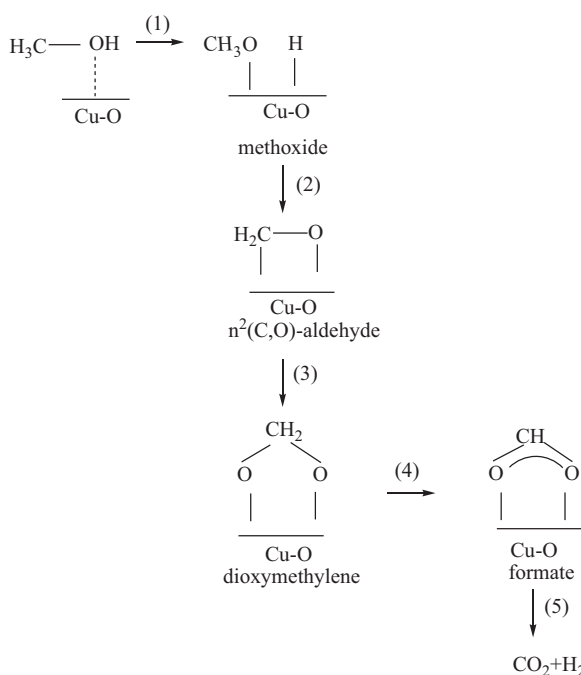


Fig. 3. ^{11}C -methanol conversion on 8CuO/SBA-15 and 8CuO/KIT-6 after different pre-adsorption procedures at 523 (a) *procedure A*: curves (1) 8CuO/SBA-15, (2) 8CuO/KIT-6, (3) used in catalysis 8CuO/KIT-6 samples; (b) *procedure B*: (1) 8CuO/SBA-15, (2) 8CuO/KIT-6 samples.



Scheme 1. Methanol decomposition on copper modified mesoporous silicas.

As a result of methanol decomposition its concentration decreases and CO (2143 cm^{-1}), formaldehyde (FA) (3470, 2816, 2754 and 1745 cm^{-1}), methane (indicated by rotational structure in the range $3560\text{--}3070\text{ cm}^{-1}$) and DME (1178 and 1120 cm^{-1}) are formed at its expense (gas phase spectra from [35] were used as reference spectra). The intensity of methanol band at 1033 cm^{-1} decreases with 20% for the calcined sample and with 35% for the reduced one as compared to the intensity of the same band before the catalytic test. This confirms the results on the catalytic test and shows that the preliminary reduction is beneficial for the catalytic activity of the sample above 680 K. We could assume the formation of DME to the activity of Lewis acid sites associated with the low coordinated cationic copper species. Note that they still exist after the reduction procedure. Such partial reduction of loaded copper oxide phase due to its high dispersion and strong interaction with the silica support was proved also by TPR and IR of probe molecules (see below). More formaldehyde is registered with the reduced sample

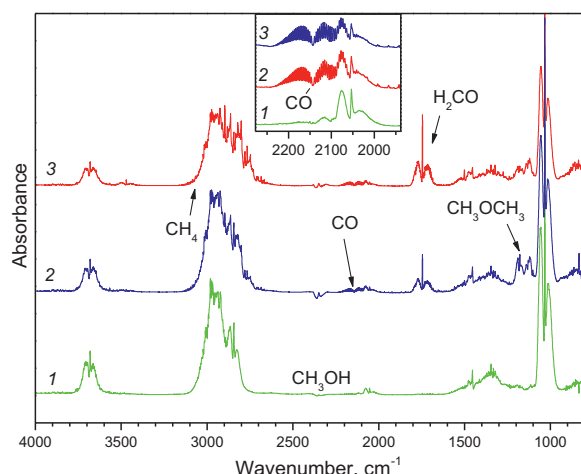


Fig. 4. Gas-phase FTIR spectra of methanol vapour (2.0 kPa) (1) and after interaction at 723 K for 15 min with 1.5%CuO/KIT-6 preliminary evacuated at 373 K (2) or preliminary reduced with H_2 at 523 K (3).

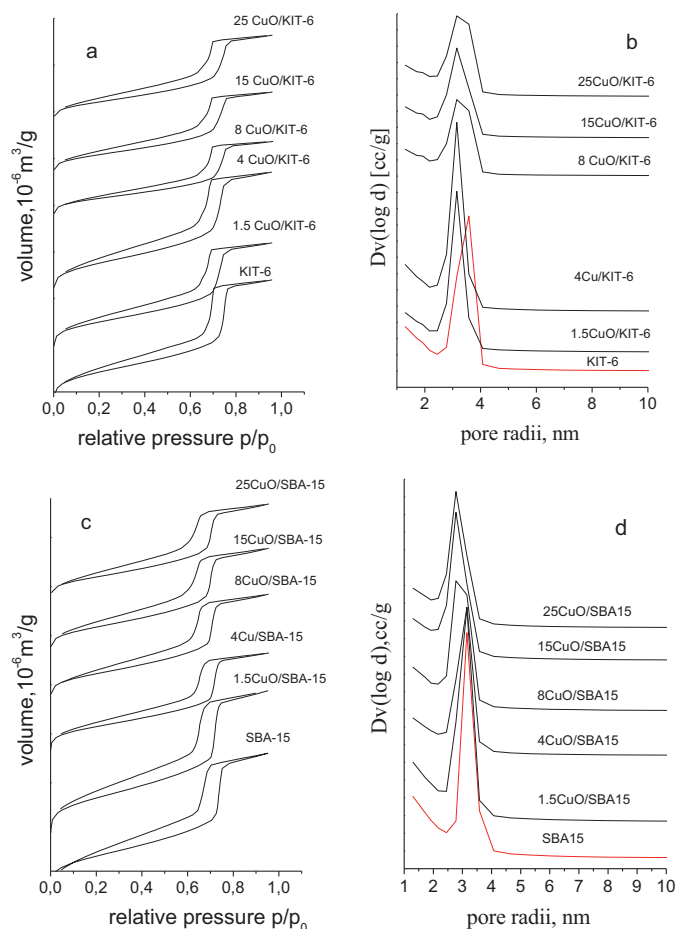


Fig. 5. Nitrogen physisorption isotherms (a and c) and pore size distribution (b and d) for KIT-6 and SBA-15 copper modifications.

while CO is almost the same with both samples. This result strongly suggests the formation of FA as a primary product from methanol decomposition both on calcined and reduced copper phase, as was proposed in **Scheme 1**.

3.2. Catalysts characterization

3.2.1. Nitrogen physisorption

Nitrogen physisorption isotherms of parent and copper modified materials are of type IV with a H1 hysteresis loop and a steep step due to capillary condensation in the 0.6–0.8 relative pressure interval which is typical for mesoporous materials with uniform cylindrical mesopores (Fig. 5). The preservation of the form of isotherms after copper modification evidences maintenance of the structure for all samples. The observed decrease in the BET surface area, total pore volume and average pore diameter after the copper modification (Table 2) indicates pore blocking to a certain degree due to the deposition of copper phase. In case of 1.5CuO/SBA-15 practically no changes in the pore characteristics and BET surface area are found in comparison with the pure SBA-15 support material. The copper phase deposition is suggested to be mainly in the pores with average radii of 3.5–4.1 nm and there are no changes in the maximum of the pore size distribution. This trend is preserved also for 4CuO/SBA-15, but the formation of copper clusters within the support pores is actively going on. These clusters seem to decrease the access of nitrogen molecules to the pores leading to a considerable decrease in both BET surface area and total pore volume. In case of 8CuO/SBA-15, a partial redistribution of the deposited phase within the porous structure occurs. This leads to an increase

Table 2

Nitrogen physisorption data of silica supports and their modifications.

Sample	A_{BET} (m ² /g)	ΔA_{BET} (%)	V_t (cm ³ /g)	ΔV_t (%)	r_p (nm)
SBA-15	845		1.21		3.2
1.5Cu/SBA-15	817	3	1.17	3	3.2
4CuO/SBA-15	555	32	0.83	29	3.2
8CuO/SBA-15	573	32	0.88	27	3.0
15CuO/SBA-15	569	33	0.87	28	2.8
25CuO/SBA-15	515	39	0.80	34	2.8
KIT-6	813		1.12		3.5
1.5Cu/KIT-6	662	18	0.94	16	3.2
4CuO/KIT-6	711	12	1.07	5	3.2
8CuO/KIT-6	453	44	0.67	40	3.3
15CuO/KIT-6	477	41	0.72	36	3.2
25CuO/KIT-6	470	42	0.75	33	3.4

A_{BET} , specific surface area by BET method; V_t , total pore volume; r_p , average pore radii.

in the dispersion and homogeneity of the copper phase distribution, which reflects at the slight increase in the BET surface area and total pore volume. As a result, pores with smaller size appear and a simultaneous decrease in the portion of the free parent ones is registered. The further impregnation steps lead to changes in the maximum of the pore size distribution due to the total blocking of the pristine pores with a simultaneous deposition of copper phase on the external surface.

As a whole, the changes in the texture parameters are larger for KIT-6 modifications than for the SBA-15 ones, indicating higher extent of incorporation of copper phase inside the pores of KIT-6. For 1.5Cu/KIT-6 samples a considerable decrease in the BET surface area and total pore volume is observed in comparison with the initial silica support. The changes in the profile of the pore size distribution and the shift in the maximum to lower sizes could be attributed to copper clusters deposition within the pores. For 4CuO/KIT-6 a partial redistribution of the copper phase within the pores occurs. This process is accompanied by an increase in the BET surface area and total pore volume due to partial release of the previously blocked pore volume (during the previous modification step). However, this affects only the larger pores (pore radii about 3.8–4.3 nm) and does not influence the maximum of the pore size distribution. At the same time the portion of pores with about 2.7–2.2 nm pore radii increases. Most significant are the changes with the BET surface area and total pore volume in case of 8CuO/KIT-6. Here, both processes of pore blocking and copper phase redistribution are observed leading to changes in the pore size distribution with the appearance of a new maximum and a substantial decrease of the initial one. The observed negligible changes in the texture characteristics for the next samples is probably due to the formation of finely dispersed and accessible to the nitrogen molecules particles predominantly on the external support surface.

So, the pore topology of the mesoporous silica support controls the copper deposition inside the mesopores of the support, and the optimal loading is about 4–8 wt.% for SBA-15 and 8–15 wt.% for KIT-6 respectively. The absence of well defined relation between the textural characteristics and the copper loading in KIT-6 modifications (Fig. 5, Table 2) indicates that the more opened 3D-porous structure facilitates the migration and agglomeration of copper phase during the preparation procedure, valid also at relatively low copper loading.

3.2.2. XRD data

The XRD patterns of all copper modifications are presented in Fig. 6. In the small angle region for SBA-15 based materials three well resolved reflections, which are indexed as (1 0 0), (1 1 0) and (2 0 0) planes of 2D-hexagonally ordered mesopores are detected (Fig. 6a) [31]. XRD patterns of KIT-6 silica based samples (Fig. 6b) show diffraction peaks assigned to (2 1 1), (2 2 2) and (4 2 0) planes of 3D-cubic mesoporous structure [32]. These observations reveal

preservation of the host matrix after the copper modification, which was demonstrated by the nitrogen physisorption measurements as well (Fig. 5). In the wide angle region of CuO/S materials, well-defined diffraction peaks at $2\theta = 35.5^\circ$, 38.5° and 48.5° , which are typical of highly crystalline CuO with average crystallite size of about 25–50 nm (Fig. 6c and d, Table 1) and monoclinic tenorite structure (JCPDS 48-1548) are detected. Such reflections are not observed for both 1.5CuO/S samples which might be due to the detection limit, and also for 4CuO/SBA-15, here probably due to the presence of highly dispersed CuO phase. This result is in accordance with the data reported in [25] where bulk CuO particles are observed for mesoporous KIT-6 silica in higher extent than in SBA-15 materials. The average particles size decreases with the copper loading increase in the range 8–25% for both silicas with a slight tendency for the formation of larger particles for the

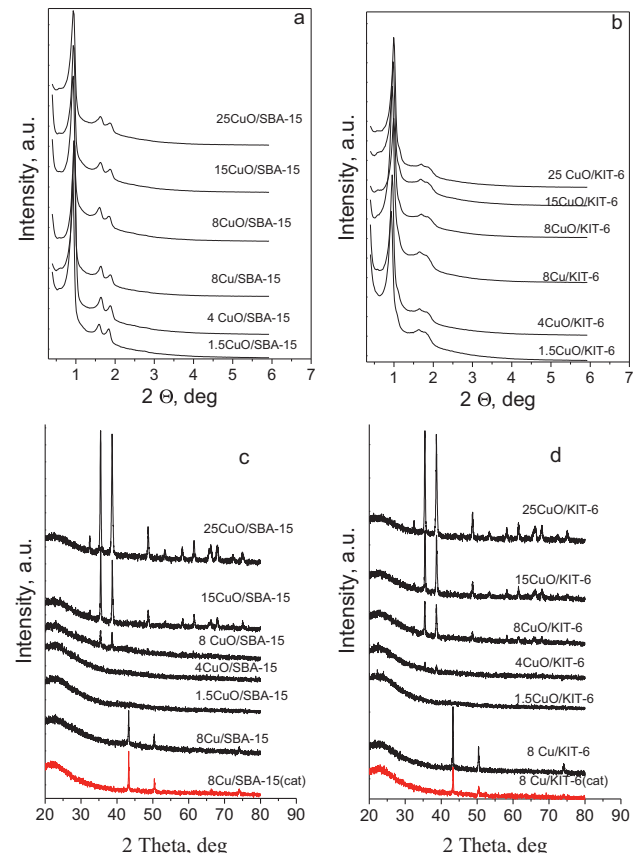


Fig. 6. XRD patterns for SBA-15 (a and c) and KIT-6 (b and d) modifications. For comparison, XRD patterns of selected samples after catalytic test (cat) are presented.

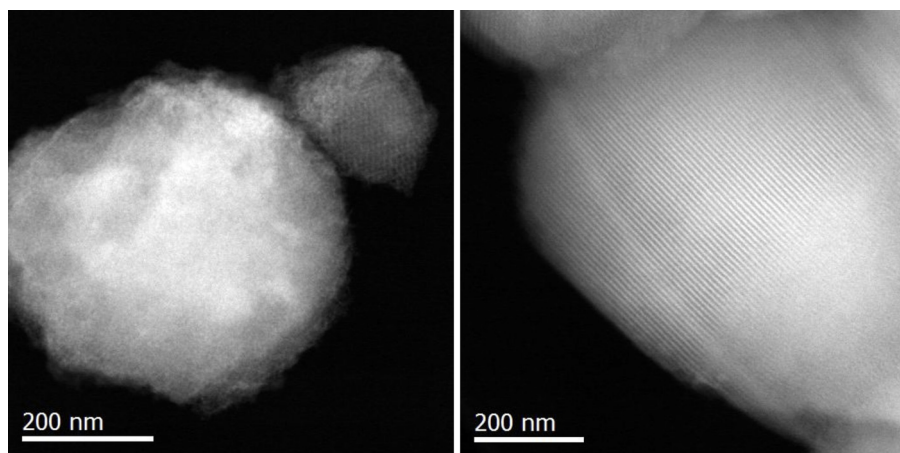


Fig. 7. HAADF-STEM images of calcined 4Cu/KIT-6 (left) and 4Cu/SBA-15 (right) samples.

KIT-6 matrix. However, the nitrogen physisorption data urge the authors to believe that the main part of loaded copper phase is finely dispersed and located into the pores particles, which size is restricted by the pore diameter. In order to describe more precisely the role of support topology on their state, TEM, UV-vis, TPR and FTIR with probe molecules investigations were carried out (see below). After the reduction, intensive reflections at $2\theta = 43.3^\circ$ along with two weak ones at $2\theta = 50.4^\circ$ and 74.1° of fcc metallic copper (JCPDS 04-0836) with average size about 40 nm (Table 1) are distinguished. The XRD patterns for the selected samples after the catalytic test (Fig. 6) clearly demonstrate changes with the morphology of copper phase. They are more significant for Cu/KIT-6 materials where about 8 nm increasing in the average particle size is found (Table 1). The observed significant decrease in the intensity of copper reflections after the catalytic test for this sample does not exclude also formation of more finely dispersed copper species with lower degree of crystallinity. These results confirm higher flexibility of copper phase into the 3D-silica matrix even during the catalytic test. We will return to this point during the discussion of TPR measurements.

3.2.3. TEM analyses

More information for the support structure as well as for the morphology and dispersion of the loaded copper phase was obtained by TEM measurements. Representative TEM images for the selected calcined samples are shown in Fig. 7. The arrays of hexagonal two dimensional ordered layers of pores are clearly identified on the images of SBA-15 loaded materials, while 3D-pore structure of a cubic repetition of the unit structure with pore mouth opening in all six directions is detected for KIT-6 samples. With the exception of 15CuO/SBA-15, no particles of copper phases could be distinguished, despite their presence within the support structure is well confirmed by EDXS-measurements (energy dispersive X-ray spectrometry). In Fig. 8 are presented selected data from the EDXS analyses for 4CuO/SBA-15 and 4CuO/KIT-6. More homogeneous distribution of copper could be assumed for the SBA-15 silica matrix, while significant deviation from the nominal calculated Si:Cu ratio was established for 4CuO/KIT-6. In contrast to the calcined samples, copper nanoparticles with almost spherical shape are distinguished for all reduced modifications. They are easier detected in the HAADF (Z-contrast) images than in the bright field images and for that reason, HAADF images are only presented in Fig. 9. Particle size distributions calculated on the base of approximately 300 particles is also shown (Fig. 9). It is clearly seen that the dominant part of the particles can be distributed within the silica porous matrix since their size is below the average pore diameter.

A slight but clear effect of particle size increase with the increase of copper loading is detected for SBA-15 materials (Table 1, Fig. 9). Such a tendency is not registered for KIT-6 counterparts, where the diameter of copper particles remains slightly smaller as compared to the SBA-15 analogues even at high copper loading.

3.2.4. TPR characterization

In order to prove the assumptions based on the spectroscopic and structural measurements, TPR-TG analyses were also performed (Fig. 10, Table 3). It is known that the method is highly sensitive to metal ion environment, which in some cases makes the interpretation of the results very complicated. The reduction of all copper SBA-15 and KIT-6 modifications proceeds above 420–450 K with pronounced weight loss with a maximum around 450–470 K and further continuous weight loss, with not defined maximum up to 700 K. Moreover, typically the reduction degree in the whole temperature interval is below 100%. Taking into account that the reduction to metallic copper for the bulk CuO occurs in one stage at about 523–553 K [22,36], we assign the observed features to the presence of copper species in different dispersion. Differences in the location of copper particles into the mesoporous matrix are not excluded, because the release of water formed during the reduction from the pores could also affect the thermo-gravimetric analyses. The low temperature DTG effect (LT), which usually prolongs up to 500 K is probably due to the reduction of well crystallized CuO particles. The weight loss in the high temperature region (HT) could be assigned to the reduction of oligomeric non-crystallized CuO species, part of them deeply located into the pores, which suppresses the water release from the pores. In agreement with [24,37] we also suggest that these species are reduced in two stages to metallic copper. The fraction, which could not be reduced in the whole investigated temperature interval probably represents isolated ions, strongly interacting with the support. On the base of this interpretation we assume that the fraction of each type of copper species is affected both from the copper loading and peculiarities of the silica structure. The observed low reduction degree and the absence of well pronounced LT maximum for 1.5CuO/S samples indicate predominant presence of oligomeric copper species, deeply located into the pores. Their partial reduction to Cu^+ is well illustrated with the observed low reduction degree (Table 3) and by the FTIR study of probe molecules (see Section 3.2.7). The presence of hardly reducible isolated ions, which fraction seems to be higher for 1.5CuO/SBA-15 as compared to 1.5CuO/KIT-6, is also assumed. The broader but well pronounced LT effect for both 4CuO/S modifications does not exclude also the presence of finely dispersed CuO crystallites,

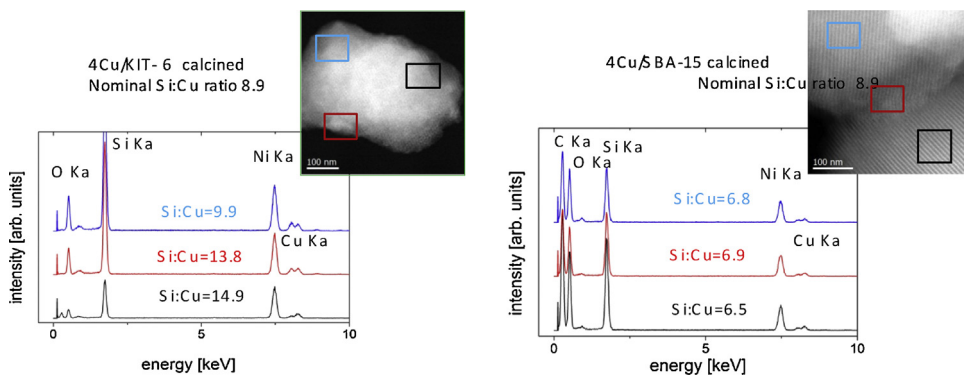


Fig. 8. EDX measurements of calcined 4 wt.% SBA-15 and KIT-6.

most of them located deeply into the pores. Their portion seems to be higher for 4CuO/KIT-6 and this correlates well with the XRD data. The tendency of CuO particles growth with increasing copper content was observed for 8 wt.% copper loading. This assumption is well illustrated with the increase of the LT effect. This effect is also shifted to lower temperatures for 8CuO/SBA-15, which evidences the presence of slightly smaller particles as compared to the KIT-6 counterpart and this is in good correlation with the XRD measurements (Table 1). Further growth of the particles with the increase of copper loading up to 15 wt.% is evidenced by the appearance of narrow LT effect, where about 75–80% of the loaded phase is reduced to metallic copper. Taking into account the XRD results (Table 1) we assign the observed shift of the LT effect for 15CuO/KIT-6 to lower temperatures than 15CuO/SBA-15 to higher exposure of CuO phase to the surface in the former material. This assumption is well supported by the nitrogen physisorption analyses (see above). The similarity in the TPR profiles for both 25CuO/S samples evidences absence of strong topology effect at this high copper loading, probably due to high extent of location of copper on the external surface. After the re-oxidation of the reduced at 523 K samples, the changes in the TPR profile clearly indicate re-dispersion of copper phase. The observed shifting of the main effect for 8CuO/KIT-6 to higher temperature with a simultaneous increase in the reduction degree could be due to the reduction of more finely dispersed particles, probably located deeply into the pores. We also re-oxidized used in the catalytic reaction 8CuO/S materials and tested them by TPR-TG. The observed shift of the TPR profiles to lower temperature as compared to the initial ones combined with about 30% decrease in the overall reduction degree clearly reveal changes in the state of copper phase during the reaction and the re-oxidation step of the used catalysts. The significantly narrow shape of the DTG profile for the used CuO/KIT-6 and in accordance with the XRD data (see above) suggest intensive processes of migration and re-dispersion

of the copper phase into the more opened 3D-structure of KIT-6. Note, that under isothermal conditions (Fig. S2), more pronounced decrease in the catalytic activity with time on stream was registered for KIT-6 modification. So, simultaneous processes of agglomeration of copper particles on the external surface and migration of finely dispersed species into the less accessible positions into the silica porous matrix could be assumed as the main reason for the catalysts deactivation. We do not exclude also the observed decrease in the reduction degree after the re-oxidation of the used catalysts to be related to the stabilization of Cu⁺ ions by the silica support which suppress their participation in the active Cu⁺–Cu⁺ or Cu²⁺–Cu⁺ redox pairs. We'll return to this point in Section 3.2.7, discussing the results of FTIR experiments with probe molecules.

3.2.5. FTIR spectra

FTIR spectra in the region of skeletal vibrations of all SBA-15 and KIT-6 modifications are shown in Fig. S4. A large and broad band situated around 3490 cm⁻¹ (not presented) is assigned to surface silanol groups and adsorbed water [38]. The three major peaks observed around 1070, 795 and 455 cm⁻¹ represents the IR absorption of Si–O–Si skeleton [39]. The two major Cu–O stretching vibrations, which typically appear at 533 cm⁻¹ and 424 cm⁻¹, are masked by the intense band corresponding to the Si–O framework at 455 cm⁻¹ [40]. The broadening at the high frequency side of the 455 cm⁻¹ band can be attributed to the presence of Cu–O band and it is more pronounced for the KIT-6 modifications with relatively high copper content. The band centred around 965 cm⁻¹ typically originates from Si–O vibrations in the Si–OH groups [41]. The slight changes in the band for all SBA-15 and KIT-6 modifications compared to the parent supports could be assigned to the copper ions interaction with surface Si–OH groups [19,30]. It is worth mentioning that this strong interaction is preserved in a high extent even after samples reduction in hydrogen (Fig. S5, dash lines).

Table 3
TPR data for the copper modifications of SBA-15 and KIT-6.

Sample	T _{ini} (K)	LT ^a (mg)	HT ^b (mg)	LT _{max} (K)	LT/HT	Reduction degree (%)
1.5CuO/KIT-6	452	0.04	0.04	–	1.0	53
1.5CuO/SBA-15	644	0.02	0.04	–	0.5	40
4CuO/KIT-6	432	0.25	0.12	457	2.1	92
4CuO/SBA-15	448	0.18	0.13	454	1.4	77
8CuO/KIT-6	443	0.54	0.12	470	4.5	82
8CuO/SBA-15	425	0.5	0.18	459	2.8	85
8Cu/KIT-6 ^c	438	0.72	0.11	467	6.5	100
8Cu/SBA-15 ^c	428	0.69	0.15	453	4.6	100
15CuO/KIT-6	443	1.13	0.15	462	7.5	85
15CuO/SBA-15	440	1.11	0.15	470	7.4	84
25CuO/KIT-6	436	1.79	0.14	463	12.7	76
25CuO/SBA-15	424	1.99	0.08	465	24.9	82

^a LT-weight loss in 400–500 K region.

^b HT-weight loss in 500–770 K region.

^c After re-oxidation at 773 K of the reduced at 523 K.

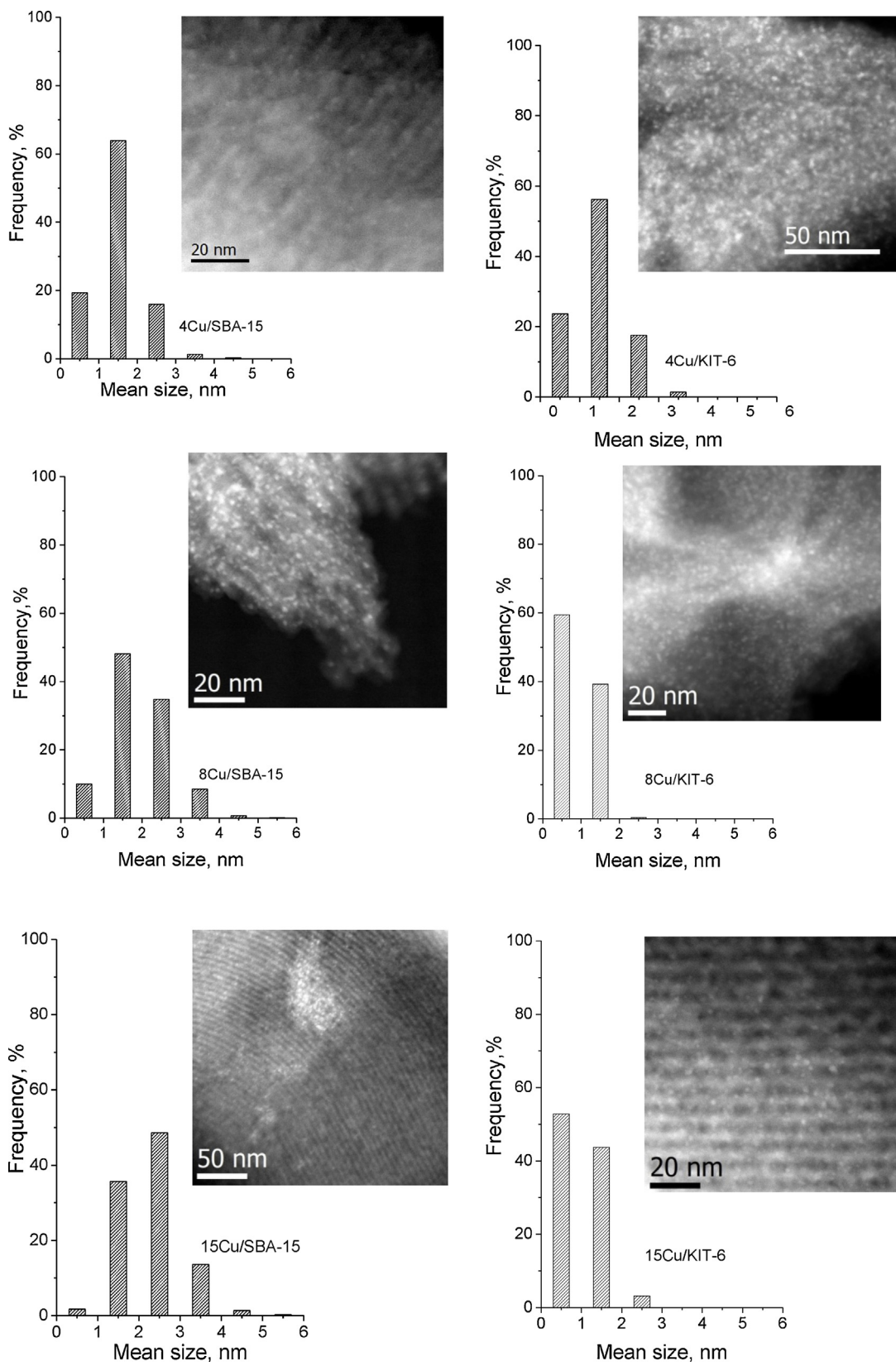


Fig. 9. Representative HAADF-STEM images and particles size distribution for selected reduced in hydrogen SBA-15 and KIT-6 modifications.

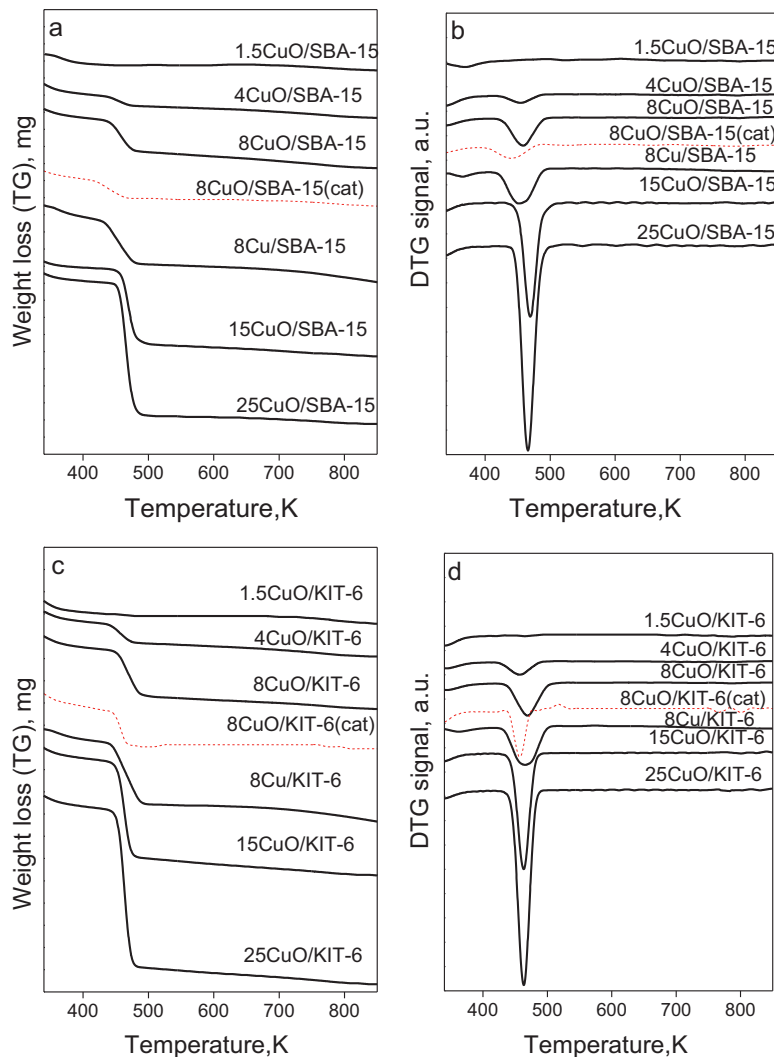


Fig. 10. TPR-TG and TPR-DTG profiles of copper modified SBA-15 (a and c) and KIT-6 (b and d) samples. For comparison the reduction profiles of selected samples, re-oxidized after the catalytic test (cat) are presented.

Supplementary material related to this article can be found, in the online version, at <http://dx.doi.org/10.1016/j.apcatb.2013.10.002>.

3.2.6. UV-vis spectra

The UV-vis spectra of both series of SBA-15 and KIT-6 supported modifications are compared in Fig. 11. The band centred at ca. 250 nm may be related to the silica matrix [42]. The increase in the intensity of this band for all modifications is assignable to metal charge transfer (CT) between the surface oxygen and isolated Cu²⁺ ions [43], which presence is also proved by FTIR of probe molecules (see below) and TPR data. The observed two bands in the 250–350 and 600–800 nm regions is due to the Cu²⁺ \leftarrow O²⁻ CT and d-d transitions, respectively of dispersed Cu²⁺ species. The peak at 680 nm corresponding to bulk CuO also appears in the spectra [25]. It is noticeable that the intensity of the shoulder at ca. 320 nm assignable to the electron charge transferring from coordination oxygen ligands to central Cu(II) ions in (Cu–O–Cu)_n oligomeric species [24] as well as the absorption in the 600–800 nm region increases with the increase of copper content, more pronounced for the KIT-6 modifications. These features suggest that copper oxide is better dispersed at low copper content on the SBA-15 mesoporous silica matrix.

3.2.7. FTIR study of probe molecules

We were not able to obtain information for copper in the case of the lowest copper content (1.5 wt.%) neither by XRD nor by TEM.

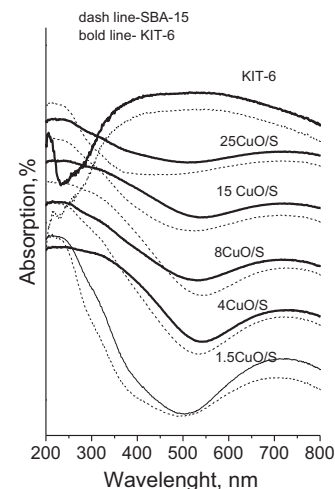


Fig. 11. UV-vis spectra of copper supported SBA-15 (dash line) and KIT-6 (bold line) modifications.

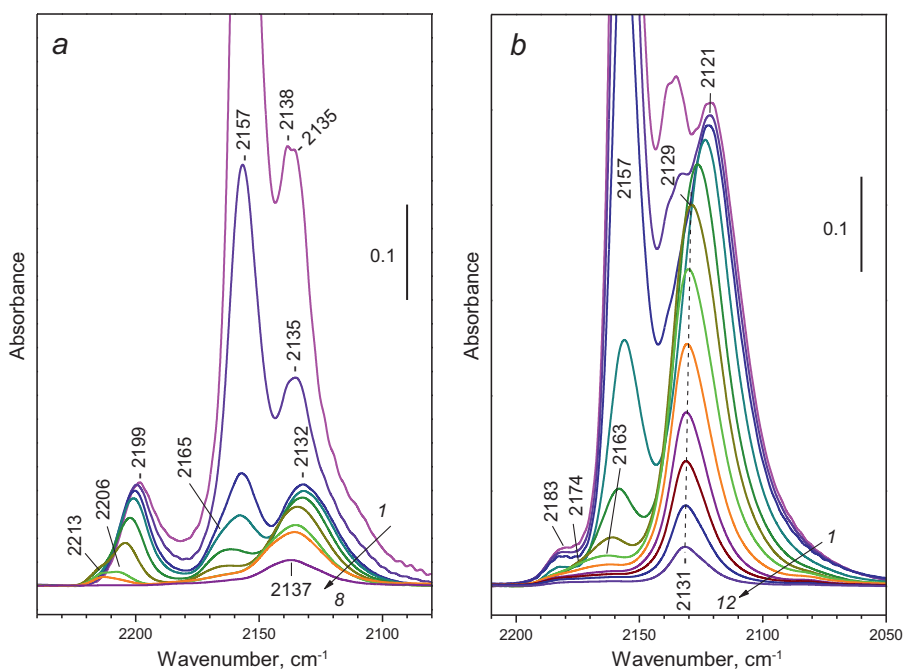


Fig. 12. FTIR spectra of CO adsorbed at 100 K on 1.5%CuO/KIT-6: activated sample (a) and sample reduced at 523 K (b). Equilibrium CO pressure of 500 Pa (1) and evolution of the spectra under dynamic vacuum at 100 K and increasing temperatures (2-12).

That is why the 1.5Cu/KIT sample was investigated by means of IR spectroscopy of probe molecules. Three different probe molecules, CO, NO and N₂, were used, because they can be very sensitive to the state of copper and can give complementary information [44]. Briefly, CO is preferentially adsorbed on Cu⁺ and Cu⁰ sites, while NO forms most stable complexes with Cu²⁺ ions. N₂ is known to form complexes with the Cu⁺ sites and the advantage of this probe is its inertness, i.e., it cannot oxidize (as NO) or reduce (as CO) the surface copper sites.

Before adsorption of the probe molecules, the non-reduced 1.5CuO/KIT sample was activated first in air and then under vacuum at 723 K or in situ reduced with hydrogen at 523 K (and evacuated at 673 K). The IR spectra of activated and reduced sample are presented in Fig. S6 (spectra 1 and 2, respectively). Both spectra are similar and typical of silica support: a band at 3743 cm^{-1} due to silanols and three broad bands within the $2000\text{--}1600\text{ cm}^{-1}$ region which characterize overtones of lattice vibrations (1961 and 1642 cm^{-1}) and a combination frequency (1864 cm^{-1}) [45].

Supplementary material related to this article can be found in the online version, at <http://dx.doi.org/10.1016/j.apcatb.2013.10.002>.

Adsorption of CO (200 Pa equilibrium pressure) at 100 K on the activated 1.5CuO/KIT-6 sample results in the appearance of three main bands at 2199, 2157 and 2138–35 cm^{−1} (Fig. 12a). Decrease of the coverage caused by evacuation results in a fast decrease in intensity of the 2157 cm^{−1} band and, at low coverage, a band at 2165 cm^{−1} becomes visible. The band at 2157 cm^{−1} is assigned to CO polarized by the silanol groups [46]. Indeed, the silanol band at 3743 cm^{−1} shifts to 3656 cm^{−1} and this shift changes in concert with the 2157 cm^{−1} band. The band at 2135 cm^{−1} is attributed to physically adsorbed CO and is thus very sensitive to the equilibrium pressure. With the decrease of this band in intensity, a new, more stable band located at 2132 cm^{−1} becomes discernible. The latter is assigned to Cu⁺–CO complexes [28,46–49]. The band at 2199 cm^{−1} characterizes carbonyls of Cu²⁺ [28,46–49]. It decreases in intensity faster than the band assigned to Cu⁺–CO complexes. At lower coverage components at 2213 and 2206 cm^{−1} are clearly visible. This can be explained by the existence of Cu²⁺–CO species formed with

two kinds of isolated Cu²⁺ cations with different electrophilicity. Thus, the results evidence the heterogeneity of the Cu²⁺ sites on the sample. Moreover, the band at 2213 cm⁻¹ partially developed at the expense of the band at 2199 cm⁻¹. This behaviour suggests that the Cu²⁺-CO species are transformed, at higher coverages, into Cu²⁺(CO)₂ geminal dicarbonyls. Similar geminal species are produced as a result of the low coordination typical of the metal cation in zeolite matrices [46]. Indeed, it was reported that cations can occupy suitable positions and be low-coordinated not only in alumina-containing, but also in siliceous materials [28]. The band at 2132 cm⁻¹ is the most stable one and decreases to about one forth of its original intensity being shifted to 2137 cm⁻¹ after 5 min evacuation at room temperature. Deconvolution of the latter shows three components at 2145, 2136 and 2125 cm⁻¹ which indicates heterogeneity of the Cu⁺ sites. These sites are formed during thermal evacuation as a result of autoreduction or reduction by organic contaminants. The band at 2165 cm⁻¹ can be attributed to the formation of some amount of Cu⁺(CO)₂ species (the corresponding ν_{as} band around 2132 cm⁻¹) [28,46,47].

The sample was reduced with H_2 at 523 K for 1 h and evacuated at 673 K. Then CO was introduced to the cell at 100 K. This led to the appearance of three main bands at 2157 cm^{-1} (H-bonded CO), 2135 cm^{-1} (physically adsorbed CO) and 2121 cm^{-1} (Fig. 12b). In addition, a weak band at 2183 cm^{-1} is observed. No bands at higher frequencies (Cu^{2+} –CO species) are detected, while the band at 2121 cm^{-1} characterizing carbonyls of reduced Cu sites is much more intense (~5 times) as compared to the non-reduced sample. Evacuation leads to decrease in intensity and disappearance of the bands at 2183 , 2157 and 2135 cm^{-1} . When the bands at 2183 and 2157 cm^{-1} disappear, weak components at 2174 and 2161 cm^{-1} become visible. The band at 2121 cm^{-1} decreases in intensity more slowly as compared to the other bands. Initially it shifts to 2129 cm^{-1} , and then stays almost at the same position. The bands at 2183 , 2174 , 2161 and 2121 cm^{-1} can be associated to polycarbonyls formed with small fraction of Cu^+ sites. Most probably the band at 2129 cm^{-1} is due to Cu^+ –CO complexes. The results show that all Cu^{2+} species are reduced by H_2 at 523 K mainly to Cu^+ . This is consistent with the relatively low reduction degree of

this sample (ca. 50%) as revealed by TPR experiment performed up to 770 K (see below). The high intensity of the band suggests high dispersion of the reduced copper.

To achieve a higher degree of reduction, the sample was reduced at 673 K. Fig. S7 shows the spectra of CO adsorbed at room temperature on the sample thus treated. The spectrum of CO adsorbed on the activated sample is also given for comparison. It contains three principal bands at 2211 and 2203 cm⁻¹, which could be assigned to two types Cu²⁺-CO species and a band at 2132 cm⁻¹ belonging to Cu⁺-CO. A careful inspection of the spectrum reveals existence of two more weak bands at 2183 and 2162 cm⁻¹. They can be attributed to very small amounts of polycarbonyls of Cu⁺. After reduction at 673 K, the bands of Cu²⁺-CO species disappear and the band of Cu⁺-CO is observed with much higher intensity. At the same time, two high frequency shoulders at 2104 and 2082 cm⁻¹ become discernible. These shoulders are assigned to CO adsorbed on high and low index planes of metal copper, respectively [49]. As one can expect, reduction at 673 K resulted in higher reduction degree as compared to reduction at 523 K. As a result, not only Cu⁺ but also Cu⁰ was formed in the former case.

Supplementary material related to this article can be found, in the online version, at <http://dx.doi.org/10.1016/j.apcatb.2013.10.002>.

We also studied NO adsorption on the 673 K reduced sample. The experiments were performed at low temperature in order to suppress the reactive NO adsorption and eventual oxidation of Cu⁰ and Cu⁺ sites. IR spectra of NO adsorbed on the activated and reduced sample are presented in Fig. S8. At low coverages the spectrum of NO on activated sample shows one intense band at ca. 1896 cm⁻¹ and two weak bands at 1810 and 1707 cm⁻¹ (spectrum 2). The band at 1896 cm⁻¹ is assigned to Cu²⁺-NO complexes [50,51]. This band is complex and consists of at least two components, at 1896 and 1869 cm⁻¹. This is in agreement with the heterogeneity of the Cu²⁺ sites revealed by CO adsorption. The couple of bands at 1810 and 1707 cm⁻¹ are characteristic of the symmetric and antisymmetric modes, respectively, of Cu⁺(NO)₂ dinitrosyls [51]. At higher coverage (spectrum b) these bands are much more intense. In this case bands due to (NO)₂ dimers and H-bonded NO are also observed (1870, 1767 cm⁻¹, respectively) [50]. The bands of dinitrosyls of Cu⁺ dominate in the spectrum of NO adsorbed on the reduced sample. Thus, NO probe molecule clearly shows existence of considerable amount of Cu⁺ sites on the sample reduced at 673 K and only traces of Cu²⁺ sites.

Supplementary material related to this article can be found, in the online version, at <http://dx.doi.org/10.1016/j.apcatb.2013.10.002>.

To prove that Cu⁺ sites were not produced as a result of oxidation of metallic copper by NO, we tested the reduced sample with N₂. Indeed, the Cu⁺-N₂ complexes were formed at low temperatures and registered at 2282 cm⁻¹ [52,53] (spectra not shown). Although adsorption of CO revealed existence of metallic copper sites, there were no bands which can be assigned to complexes of these sites with NO or N₂. Therefore, we can conclude that these probe molecules are “blind” towards Cu⁰ sites.

As it was already noticed, at temperatures above 680 K the reduced 1.5Cu/KIT sample is more catalytically active than the non-reduced sample. In order to highlight the reasons for this, we characterized the state of copper in the reduced and non-reduced sample after their interaction with methanol at 723 K followed by evacuation at the same temperature. Before this, in two separate experiments the sample was (i) evacuated at 373 K or (ii) reduced with H₂ at 523 K and evacuated at the same temperature. The resulting spectra (2 and 3, respectively) after these two treatments were very similar (Fig. S6). In both cases, bands due to metoxy groups bonded to Si (3033, 2996, 2972, 2957, 2924, 2855,

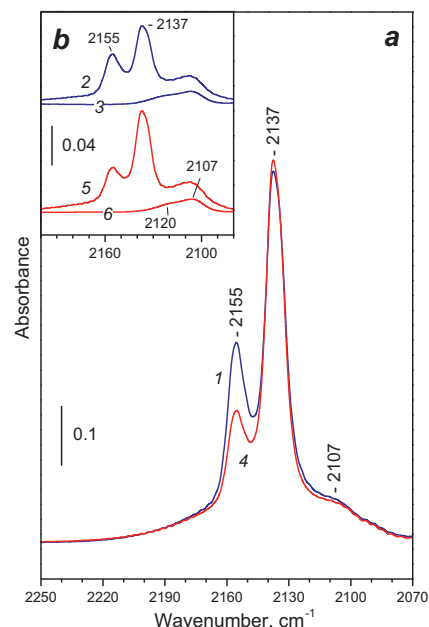


Fig. 13. FTIR spectra of CO adsorbed at 100 K on 1.5%CuO/KIT-6: methylated-nonreduced sample (spectra 1–3) and methylated-reduced sample (spectra 4–6). Equilibrium CO pressure of 500 Pa (spectra 1 and 4) and after evacuation at 100 K for 2 (spectra 2 and 5) and for 5 min (spectra 3 and 6).

1471, 1463 cm⁻¹) were detected [54,55]. Indeed, Si-OCH₃ can be stable at temperatures above 673 K [56].

After the above described pretreatments the samples were tested by CO at 100 K. The spectra of CO adsorbed on reduced and non-reduced sample are similar (Fig. 13). At high CO coverage, a band of H-bonded CO (2155 cm⁻¹) and a band of physically adsorbed CO (2137 cm⁻¹) were observed. At intermediate coverages, bands at 2120 and 2107 cm⁻¹ due to copper carbonyls were revealed (see the inset in Fig. 13). Probing the samples by NO and N₂ did not show existence of any Cu⁺ sites. This is an indication that Cu⁺ sites were blocked by metoxy species or did not exist. Therefore we assign the two bands at 2120 and 2107 cm⁻¹ to different Cu⁰ sites on the surface of metal particles. The results show that the chemical state of copper after interaction with methanol at 723 K is practically the same, independently of the fact whether the sample was or was not pre-reduced with hydrogen. Probably, the difference in activity is due to different distribution of copper in the porous structure of the support. Indeed, comparison of the spectra of CO adsorbed at high coverage on methylated-reduced and methylated-nonreduced sample at high coverage show that the band of physically adsorbed CO is observed with lower intensity in the latter case suggesting restricted accessibility of the active surface.

4. Concluding remarks

The formation of catalytically active sites in copper supported mesoporous silica materials is a complex process, which proceeds not only during the modification and activation procedure, but also could be influenced by the reaction medium. XRD, UV-vis and TEM analyses evidence that the modified incipient wetness impregnation technique provides good opportunity for the preparation of uniform and finely dispersed CuO or metallic copper nanoparticles even at high copper loading. This ensures much higher catalytic activity, especially at high temperature, for the samples prepared by MWI method in comparison with the catalysts obtained by the conventional incipient wetness impregnation technique. The catalysts obtained by MWI method exhibit lower initial catalytic

activity but improved stability, which provides even better catalytic activity with time on stream, as compared to the commercial one. Nitrogen physisorption analyses and TEM images clearly demonstrate that the stabilization of copper phase in a highly dispersed state for the materials obtained by MWI method even after their pre-treatment in hydrogen is favoured by predominant location of copper nanoparticles into the porous structure. This tendency is more pronounced for the more opened 3D-structure of KIT-6. However, at relatively low copper content, the facilitated migration of the supported copper phase into this structure results in segregation of larger copper particles on the external silica surface.

FTIR of probe molecules clearly demonstrated that both Cu^0 and Cu^{2+} could be included in the catalytic active sites for methanol decomposition. The catalytic experiments under trace surface coverage with ^{11}C -radiolabelling methanol support heterogeneity of copper. The selective coverage of catalyst surface with ^{11}C -methanol indicates that KIT-6 structure facilitates the formation of larger portion of copper sites strongly adsorbing CH_3OH as compared to SBA-15. These sites seem to provide better catalytic activity in methanol decomposition. Analyzing the FTIR of probe molecules and TPR data we attribute the weaker adsorption sites to isolated copper ions. They dominate at copper loading of about 1.5 wt.% for both silica matrices and partially transform to Cu^+ under the reduction conditions. It is not excluded the stabilization of Cu^+ ions by the silica support to suppress their participation in active $\text{Cu}^0\text{--Cu}^+$ and $\text{Cu}^{2+}\text{--Cu}^+$ redox pairs. This provokes decrease in the catalytic activity in methanol decomposition to CO and hydrogen after the reduction of samples with hydrogen or by the influence of the reaction medium.

The absence of clear relationship between the catalytic activity and copper crystallite size even after the elimination of the role of copper oxidation state, which could be changed during the reaction by the influence of the reaction medium, points out the dominant effect of the location of copper particles into the porous structure. The careful analyses of the nitrogen physisorption, TEM-EDXS, TPR and FTIR of probe molecules results indicate that the pore topology of the mesoporous support controls significantly not only the dispersion of active copper phase but also its accessibility to the reactants. Therefore, the optimal copper loading depends on the support pore topology and for the MWI preparation procedure, the highest catalytic activity was achieved at 8 and 15 wt.% copper loading, respectively, for the SBA-15 and KIT-6 support.

Acknowledgements

Financial support of Bulgarian Academy of Science; Bulgarian Ministry of Education, project BG051PO001-3.3-05/000; National Scientific Fund of Bulgarian Ministry of Education, Projects DTK 02/64 and DFNI-E01/7/2012 is gratefully acknowledged.

References

- [1] G. Marbán, A. López, I. López, T. Valdés-Solís, *Appl. Catal. B: Environ.* 99 (2010) 257–264.
- [2] O.A. Kutlar, A.T. Calik, H. Arslan, T. Özaktas, F. Karaosmanoglu, *World Renewable Energy Congress VI*, 2000, p. 2508.
- [3] M. Zhao, X. Li, L. Zhang, C. Zhang, M. Gong, Y. Chen, *Catal. Today* 175 (2011) 430–434.
- [4] J. Vancoillie, J. Demuynck, L. Sileghem, M. Van De Ginste, S. Verhelst, *Int. J. Hydrogen Energy* 37 (2012) 9914–9924.
- [5] L. Yi-jun, Y. Wen-juan, H. Shuang-hui, W. Bao-wei, *J. Fuel Chem. Technol.* 40 (6) (2012) 698–706.
- [6] M. Cimenti, J.M. Hill, *J. Power Sources* 195 (2010) 54–61.
- [7] W.H. Cheng, *Appl. Catal. A: Gen.* 130 (1995) 13–30.
- [8] W.H. Cheng, C.Y. Shiao, T.H. Liu, H.L. Tung, H.H. Chen, J.-F. Lu, C.C. Hsu, *Appl. Catal. B: Environ.* 18 (1998) 63–70.
- [9] M. Manzoli, A. Chiorino, F. Bocuzzi, *Appl. Catal. B: Environ.* 57 (2004) 201–209.
- [10] G.J. Millar, C.H. Rochester, K.C. Waugh, *J. Chem. Soc. Faraday Trans.* 87 (1991) 2795–2804.
- [11] D.B. Clarke, D.K. Lee, M.J. Sandoval, A.T. Bell, *J. Catal.* 150 (1994) 81–93.
- [12] I.A. Fisher, A.T. Bell, *J. Catal.* 184 (1999) 357–376.
- [13] T.P. Minyukova, I.I. Simentsova, A.V. Khasin, N.V. Shterter, N.A. Baronskaya, A.A. Khassin, T.M. Yurieva, *Appl. Catal. A: Gen.* 237 (2002) 171–180.
- [14] J. Greeley, M. Mavrikakis, *J. Catal.* 208 (2002) 291–300.
- [15] L. Domokos, T. Katona, A. Molnar, A. Lovas, *Appl. Catal. A: Gen.* 142 (1996) 151–158.
- [16] Y. Morikawa, *Adv. Catal.* 39 (1993) 303–327.
- [17] E.D. Guerreiro, O.F. Gorri, L.A. Arrua, *Appl. Catal. A: Gen.* 165 (1997) 259–271.
- [18] E.D. Guerreiro, O.F. Gorri, G. Larsen, L.A. Arrúa, *Appl. Catal. A: Gen.* 204 (2000) 33–48.
- [19] N.B. Linder, R. Besse, F. Audonnet, S. LeCaer, J. Deschamps, M.I. Clerc, C.A. Simionescu, *Microporous Mesoporous Mater.* 132 (2010) 518–525.
- [20] O. Karvan, H. Atakül, *Fuel Process. Technol.* 89 (2008) 908–915.
- [21] A. Yin, X. Guo, W. Dai, H. Li, K. Fan, *Appl. Catal. A: Gen.* 349 (2008) 91–99.
- [22] K.M. Parida, D. Rath, *Appl. Catal. A: Gen.* 321 (2007) 101–108.
- [23] L.-F. Chen, P.-J. Guo, L.-J. Zhu, M.-H. Qiao, W. Shen, H.-L. Xu, K.-N. Fan, *Appl. Catal. A: Gen.* 356 (2009) 129–136.
- [24] L. Chmielarz, P. Kustrowski, R. Dziembaj, P. Cool, E.F. Vansant, *Appl. Catal. B: Environ.* 62 (2006) 369–380.
- [25] A. Kong, H.W. Wang, X. Yang, Y.W. Hou, Y.K. Shan, *Microporous Mesoporous Mater.* 118 (2009) 348–353.
- [26] C.-H. Tu, A.-Q. Wang, M.-Y. Zheng, X.-D. Wang, T. Zhang, *Appl. Catal. A: Gen.* 297 (2006) 40–47.
- [27] Z. Wu, Y. Wang, W. Huang, J. Yang, H. Wang, J. Xu, Y. Wei, J. Zhu, *Chem. Mater.* 19 (2007) 1613–1625.
- [28] K. Hadjiivanov, T. Tsoncheva, M. Dimitrov, C. Minchev, H. Knözinger, *Appl. Catal. A: Gen.* 241 (2003) 331–340.
- [29] T. Tsoncheva, V. Dal Santo, A. Gallo, N. Scotti, M. Dimitrov, D. Kovacheva, *Appl. Catal. A: Gen.* 406 (2011) 13–21.
- [30] A. Patel, P. Shukla, T. Rufford, S. Wangc, J. Chena, V. Rudolph, Z. Zhu, *Appl. Catal. A: Gen.* 409–410 (2011) 55–65.
- [31] M. Choi, W. Heo, F. Kleitz, R. Ryoo, *Chem. Commun.* (2003) 1340–1341.
- [32] F. Kleitz, S.H. Choi, R. Ryoo, *Chem. Commun.* (2003) 2136–2137.
- [33] S.T. Yong, K. Hidajat, S. Kawi, *Catal. Today* 131 (2008) 188–196.
- [34] E. Sarkadi-Priboczki, T. Tsoncheva, L. Ivanova, *Can. J. Chem.* 87 (2009) 478–485.
- [35] <http://webbook.nist.gov>
- [36] M. Hartmann, S. Racouchot, C. Bischof, *Microporous Mesoporous Mater.* 27 (1999) 309–320.
- [37] X.-Y. Hao, Y.-Q. Zhang, J.-W. Wang, W. Zhou, C. Zhang, S. Liu, *Microporous Mesoporous Mater.* 88 (2006) 38–47.
- [38] S. Suvanto, T.A. Pakkanen, J. Mol. Catal. A: Chem. 164 (2000) 273–280.
- [39] T.C. Sheng, S. Lang, B.A. Morrow, I.D. Gay, *J. Catal.* 148 (1994) 341–347.
- [40] A.B. Kuzmenko, D. van der Marel, P.J.M. van Bentum, E.A. Tishchenko, C. Presura, A. Bush, *Phys. Rev. B* 63 (2001) 094303–094312.
- [41] X. Wang, *J. Porous Mater.* 18 (2011) 623–630.
- [42] Y. Itho, S. Nishiyama, S. Tsuruya, M. Masai, *J. Phys. Chem.* 98 (1994) 960–967.
- [43] L.P. Wang, A.G. Kong, B. Chen, H.M. Ding, Y.K. Shan, M.Y. He, *J. Mol. Catal. A: Chem.* 230 (2005) 143–150.
- [44] G. Ertl, H. Knözinger, F. Schüth, J. Weitkamp (Eds.), *Handbook of Heterogeneous Catalysis*, 2nd ed., Wiley VCH, Weinheim, 2008.
- [45] T. Pieplu, F. Poignant, A. Vallet, J. Saussey, J.-C. Lavalle, G. Mabilon, *Stud. Surf. Sci. Catal.* 96 (1995) 619–626.
- [46] K. Hadjiivanov, G. Vayssilov, *Adv. Catal.* 47 (2002) 307–511.
- [47] A. Gallo, T. Tsoncheva, M. Marellia, M. Mihaylov, M. Dimitrov, V. Dal Santo, K. Hadjiivanov, *Appl. Catal. B: Environ.* 126 (2012) 161–171.
- [48] G. Busca, U. Costantino, F. Marmottini, T. Montanari, P. Patrono, F. Pinzari, G. Ramis, *Appl. Catal. A-Gen.* 310 (2006) 70–78.
- [49] N. Sheppard, T.T. Nguyen, in: P.J. Clarke, R.E. Hester (Eds.), *Advances in Infrared Raman Spectroscopy*, vol. 5, Wiley, New York, 1978, pp. 67–148.
- [50] K. Hadjiivanov, *Catal. Rev. Sci. Eng.* 42 (2000) 71–144.
- [51] J. Valyon, W. Keith Hall, *J. Phys. Chem.* 97 (1993) 1204–1212.
- [52] C. Lamberti, S. Bordiga, M. Salvalaggio, G. Spoto, A. Zecchina, F. Geobaldo, G. Vlaic, M. Bellatrecchia, *J. Phys. Chem. B* 101 (1997) 344–360.
- [53] A. Itadani, Y. Kuroda, M. Nagao, *Microporous Mesoporous Mater.* 70 (2004) 119–126.
- [54] B.A. Morrow, *J. Chem. Soc. Faraday Trans. 1* (70) (1974) 1527–1545.
- [55] B.A. Morrow, *J. Phys. Chem.* 81 (1977) 2663–2666.
- [56] J. Rasko, J. Bontovics, F. Solymosi, *J. Catal.* 146 (1994) 22–33.